Surface-Wave Launchers for Beam Steering and Application to Planar Leaky-Wave Antennas

Symon K. Podilchak, *Member, IEEE*, Al P. Freundorfer, *Senior Member, IEEE*, and Yahia M. M. Antar, *Fellow, IEEE*

***Abstract*—A linear array of surface-wave launchers (SWLs) is presented for surface-wave (SW) beam steering on a grounded dielectric slab (GDS). Specifically, a two-element array of directive Yagi-Uda like SWL antennas (operating between 21–24 GHz) is investigated. By varying the relative phase difference between SWL elements, the excited SW field distribution can be steered. In addition, a six-element linear array of SWLs with nonuniform weighting is also presented. If metallic gratings are placed on top of the GDS, the bound SW mode can be transformed into a radiated leaky-wave (LW) mode and directive beam patterns can be generated in the far field. A specific elliptical grating configuration is also investigated demonstrating single frequency cylindrical-sector LW beam steering. These slotted SWL arrays can be useful for novel SW beam scanning designs, millimeter wave power distribution systems and new LW antennas.**

***Index Terms*—Leaky-wave (LW), leaky-wave antenna (LWA), surface-wave (SW), surface-wave launcher (SWL).**

I. Introduction

RECENTLY surface-wave launcher (SWL) antennas have been recognized as a practical feeding technique for planar leaky-wave antennas (LWAs). In these applications, a bound cylindrical TM_0 surface-wave (SW) mode is excited on a grounded dielectric slab (GDS) and propagation occurs along the guiding surface. Ground plane slots define these SWLs and the slotted configurations act as magnetic dipole sources for the 2-D LWAs [1]–[4]. Furthermore, these SWL antennas can be placed in an array achieving SW beam scanning. By varying the relative phase difference between SWL elements, the generated SW field pattern can be scanned. Such a SWL array configuration has applications for novel single frequency leaky-wave (LW) beam steering antennas [5], [6].

This paper investigates a two-element linear array of directive Yagi-Uda like SWL antennas [1]–[3]. The generated SW field pattern is steered by changing the relative phase difference ($\delta = \Phi_2 - \Phi_1$) between SWL elements as shown in Fig. 1. The slotted SWLs are spaced $d = (\lambda^{SW}/2)$ apart on the bottom of the GDS and a TM_0 SW mode is excited on top of the guiding surface. The substrate properties and height ($\epsilon_r = 10.2$, $\tan\delta = 0.0023$, and $h = 1.27$ mm) characterize the SW phase constant ($\beta^{SW} = (2\pi/\lambda^{SW}) = 2k_0$ at 22 GHz) of the guided-wave mode [7]. Sections II and III explain the operation of a single SWL element and arrayed configuration, respectively.

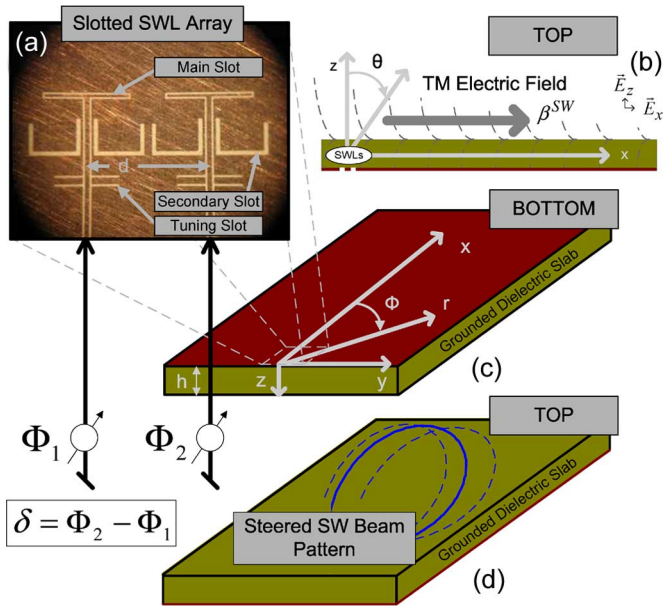

Fig. 1. The two-element array of SWLs considered in this work. (a) The slotted magnetic dipole sources are appropriately placed apart ($d = \lambda^{SW}/2$) and each element is described by a main radiating driven slot, tuning elements, and secondary reflector slots. (b) Generated TM_0 SW mode that is bound to the GDS (top). (c) The SWLs are placed on the edge of a ground plane (bottom). (d) By variation in the relative phase difference between SWL elements ($\delta = \Phi_2 - \Phi_1$) the SW beam pattern can be steered.

Furthermore, a six-element linear array of SWLs with nonuniform weighting is also presented. This extension of the two-element design suggests that known array theory can be applied to other complex SWL configurations. Section IV describes a binomial weighting distribution for minimal SW sidelobe levels [8] while calculated weights are determined to direct the main SW beam using the Godara method [9].

To observe the SW beam patterns generated by the SWLs the evanescent field distribution on top of the GDS was measured [10]. A near-field probe was translated along an arc centered at the SWL elements. The measured fields along this arc give indication of the SW field distributions on the guiding surface and thus can define the SW beam pattern. Section V further describes this measurement technique.

By the addition of periodic metallic gratings, on top of the GDS, a partially reflecting surface (PRS) is defined and LWs can be excited [3]–[6], [10]–[17] and steered along the guiding surface, as shown in Fig. 2. A continuous elliptical grating configuration is investigated in Section VI. Thus by using the afore-

Manuscript received March 29, 2008; revised August 28, 2008. Current version published March 20, 2009.

The authors are with the Electrical Engineering Departments of the Royal Military College of Canada (RMC) Kingston, ON K7K 7B4 Canada and also with Queen's University, Kingston, ON K7L 3N6, Canada (e-mail: antar-y@rmc.ca).

Color versions of one or more of the figures in this paper are available online at http://ieeexplore.ieee.org.

Digital Object Identifier 10.1109/TAP.2008.2011248

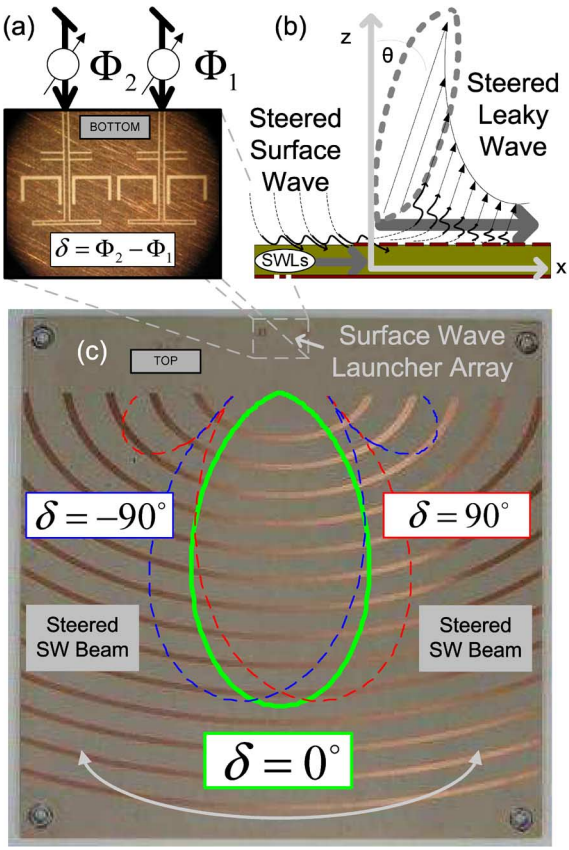

Fig. 2. By variation in δ the two-element SWL array (bottom) cylindrical TM_0 SWs can be steered on the GDS (top) and with appropriate boundary conditions LWs can be generated. (a) Two-element SWL array. (b) By the addition of a continuous strip PRS cylindrical-sector LWs can be excited and thus directive beam patterns can be steered in the far field. (c) The elliptical grating configuration and an illustration of the steered SW beam patterns (top), produced by the SWL array, for $\delta = 0^\circ$ and $\delta = \pm 90^\circ$.

mentioned SWL array, controlled SW beam steering can dictate the region of LW field excitation and thus direct beam patterns in the far field for single frequency beam steering [5], [6].

II. Individual SWL Elements for Planar SW Excitation

To excite the dominant TM_0 SW mode on the GDS, coplanar waveguide transmission line fed SWLs were utilized. These Yagi-Uda like directive SWLs were realized by half wavelength slots in the ground plane. Such slots have magnetic field distributions which can inductively couple to the dominant TM_0 SW mode of the GDS. Essentially, the single SWL element is described by a main radiating slot (length of 1.92 mm) with two secondary reflector (individual length of 2.75 mm) and four tuning elements (individual length of 0.65 mm), as shown in Fig. 1(a). Feeding the SWL with a coplanar waveguide transmission line realizes a planar SW excitation mechanism [1]–[6], [17].

A. Directive SWL Operation

Dimensions of the SWL are shown in Fig. 3. Forward SW directivity is achieved by using the secondary reflector slots (so

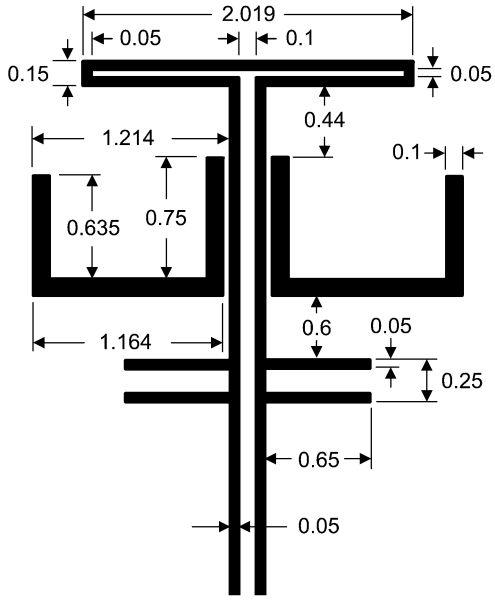

Fig. 3. Physical dimensions of the single directive SWL. The coplanar waveguide transmission line feed has a center strip and gap width of 0.1 and 0.05 mm, respectively.

that the magnetic current on the slots leads the current on the main slot by 90°). Consequently, the SW fields add constructively at the main radiating slot. At the secondary reflector slots, the field distributions add destructively and, hence, cancel. This results in a directive SW propagating in the $+\hat{x}$ direction.

Generally, reflector based SWLs have a reflector that is slightly longer than the main slot [2]. The secondary slots were folded to achieve side by side placement for the desired arrayed configuration. Without such folding the SWL elements would physically touch. This is unwanted. In fact, minimum mutual coupling is required [8] between the SWLs for efficient arrayed operation.

By changing the lengths of the tuning slots (or shorted stubs for the coplanar waveguide transmission line) the input impedance of the SWLs can be matched to 50 Ω acting as shorted stubs for the coplanar waveguide transmission line. Furthermore, the reflector slots act as a controlled element, adjusting the directivity in the forward $+\hat{x}$ direction at the cost of decreasing the operating bandwidth of the SWLs [2].

B. Generated SW Beam Pattern

To characterize the generated SW field distributions along the guiding surface, measurements were completed and compared against simulated and analytical values for the single SWL element. Simulations were performed along the air-dielectric interface of an infinite slab to determine field strength values. A commercially available full-wave solver was used, i.e., Ansoft's High Frequency Structural Solver (HFSS). Analytical values were obtained using (1) and results are in good agreement. Fig. 4 illustrates the directive SW beam pattern in the forward $+\hat{x}$ direction. The $\vec{H}_y^{SW}(\phi)$ field distribution on the slab is directly proportional to the magnitude of the SW beam pattern on the

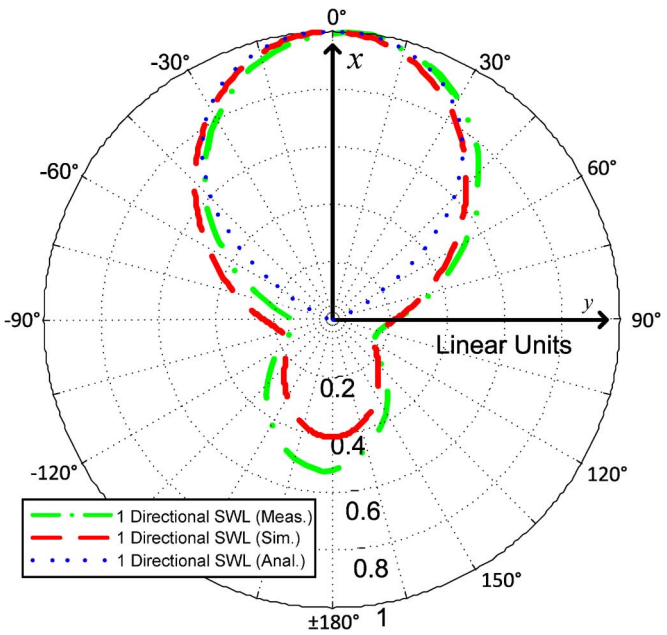

Fig. 4. Measured, simulated and analytical SW field distribution for the directive SWL (normalized and shown in linear units). To measure and simulate the single SW beam an individual SWL element was placed at the center of a GDS. Furthermore, the analytical SW beam pattern should be symmetric in both the $\pm\hat{x}$ directions. Since the investigated directive SWL has only a main beam in $+\hat{x}$ direction, the analytical SW beam was ignored for the $-\hat{x}$ direction.

guiding surface and is described in [1] as a sinusoidal-Gaussian function

$$\left|\vec{H}_y^{SW}(\phi)\right| \propto \frac{1}{\sqrt{|\cos\phi|}} \exp\left\{-\left(\frac{\beta^{SW} l \tan\phi}{2}\right)^2\right\} \quad (1)$$

where β^{SW} is the phase constant of the SW propagating along the guiding surface, l is the physical length of the main radiating slot and ϕ defines the angle along the azimuth. For this design, the SW propagation constant (β^{SW}) is dictated by the electrical properties of the GDS ($\epsilon_r = 10.2$, $\tan\delta = 0.0023$ and $h = 1.27$ mm).

When compared to simulated and measured values the analytical model provides a good agreement in the forward $+\hat{x}$ direction only, since (1) takes into account the SW generated by the main radiating slot and ignores the secondary effects of the tuning elements and reflector slots. Furthermore, a significant amount of back lobe radiation is shown in the measured and simulated values due to the coplanar waveguide transmission line feed, tuning elements and parasitic reflector slots. The analytical SW beam pattern of (1) excludes these second order effects and thus explains the observed deviation.

Measurement and analytical results for the SW beam patterns are shown at 22 GHz, while the simulated pattern was determined at 24 GHz. Maximum field strength values were observed for these two frequencies. The shift is likely due to the optimal performance (minimum reflection loss values) of the individual SWL element as shown in Fig. 5. Deviations are a likely result of substrate variations, fabrication tolerances and difficulty in modeling the metal thicknesses near the slots due to microfabrication.

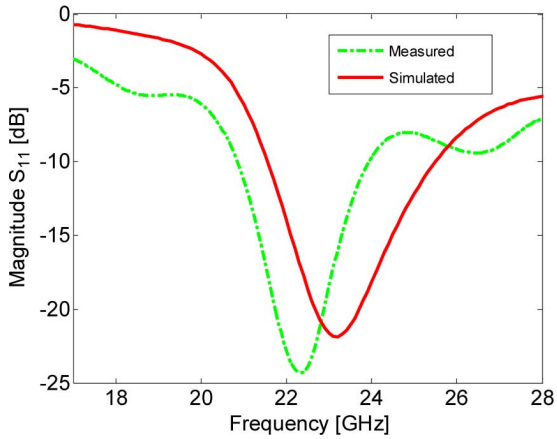

Fig. 5. Reflection coefficient of the directive SWL antenna. Simulation and measured results are in good agreement. Measured results suggest that the SWL has a reflection loss greater than 10 dB from 21 to 24 GHz.

C. Single SWL Performance

Measurements were completed for a single directive SWL and a reasonable reflection coefficient was observed. The reflection coefficient is less than -10 dB from 21 to 24 GHz as shown in Fig. 5. The SWLs were designed for a 50-Ω system impedance and, thus, were optimized for a good match to the coplanar waveguide transmission line feed. Simulation and measured results are in good agreement. A slight shift is observed between the measured and simulated values as discussed in the last section.

III. An Array of SWLs

Two directive SWLs were embedded at the edge of the ground plane of the dielectric slab, with an element spacing of $d = (\lambda^{SW}/2) = 2.971$ mm to minimize SW sidelobe levels. Measurements of the SW beam patterns were conducted at 22 GHz, while simulated values were collected at 24 GHz. Analysis was completed at these two distinct frequencies due to the observed minimal reflection loss values for the individual SWL elements within the array ($S_{11} < -20$ dB at 22 GHz [24 GHz] for measured [simulated]) as shown in Fig. 6 and as previously discussed for the single SWL element. The SW beam scanning capabilities of the array were also investigated by using the measurement setup described in Section VI. Results were compared to simulated values and to analytical equations, all are in good agreement.

A. Performance Analysis of the Two-Element Array

A performance measure of the array can be the isolation between elements and the reflection loss of a single element within the array. Measured and simulated values are compared in Fig. 6. The reflection losses are below 20 dB for both the measured and simulated values. Furthermore, the coupling between each element is below 15 dB. These values may be reasonable for such an arrayed configuration of directive SWLs.

B. Array Factor and Total SW Beam Pattern

The SW field pattern generated by the two-element array of SWLs can be determined by standard array theory. The element

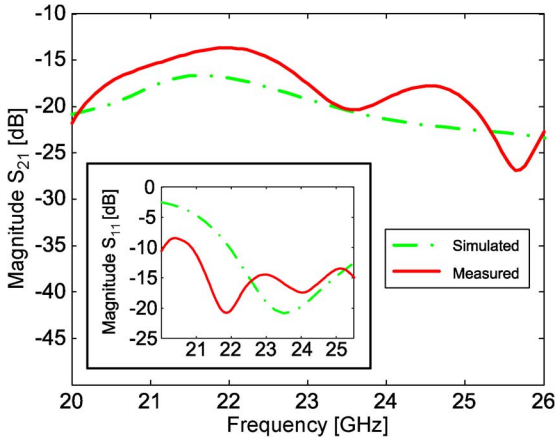

Fig. 6. Measured and simulated mutual coupling (S_{21}) between two elements of the directive SWL array. Since the two-element array is symmetric it is expected that $|S_{21}| = |S_{12}|$. The simulated and measured reflection loss (S_{11}) of a single directive SWL (in the two-element array) is also shown. As expected results are similar to the single SWL element.

factor describing the generated SW field pattern on the guiding surface can be described by (1). If the SWL elements are placed along the $\hat{y}$ axis (as shown in Figs. 1 and 2) the array factor can be derived from [8]

$$AF(\phi) = \frac{\sin\left[\beta^{SW} d\cos\left(\phi - \frac{\pi}{2}\right) + \delta\right]}{\sin\left[\frac{1}{2}\left(\beta^{SW} d\cos\left(\phi - \frac{\pi}{2}\right)\right) + \delta\right]} \tag{2}$$

where d is the spacing and δ is the relative phase difference between SWLs elements. Thus, the total magnitude of the SW field distribution on the aperture $A(\phi)$ can be determined by the multiplication of the array factor $AF(\phi)$ and SW field pattern $|\vec{H}_y^{SW}(\phi)|$ generated from a single SWL element

$$A(\phi) = AF(\phi)\left|\vec{H}_y^{SW}(\phi)\right|. \tag{3}$$

C. Measured SW Beam Patterns

The directive SW beam patterns generated by the two-element array of SWLs are shown in Figs. 7–10. Measured, simulated, and analytical beam patterns are in good agreement. The polar plot of Fig. 7(a) illustrates the SW beam pattern with no phase difference between SWL elements (shown in linear units). The back lobe SW radiation (generated by coplanar waveguide transmission line feed and tuning and reflector slots) was simulated by placing the SWLs at the center of the slab as shown in Fig. 7(b). Futhermore, Figs. 8–10 display the normalized beam pattern in dB with $\delta = 30°$, $60°$ and $90°$.

The SW beam patterns can be further steered by turning on or off the left or right SWLs within the array. Results illustrate the SW beam pattern on the GDS with the left SWL turned on as shown in Fig. 11. Essentially, when the left or right SWL elements are independently turned on or off, SW power is reflected away from the unexcited SWL antenna. Similar results are expected if the right SWL is on and the left SWL is off (SW beam pattern can be steered to $\phi = +60°$) due to the symmetry of the SWL array. Thus, by turning on or off the left or right SWLs, extended SW beam scanning is possible.

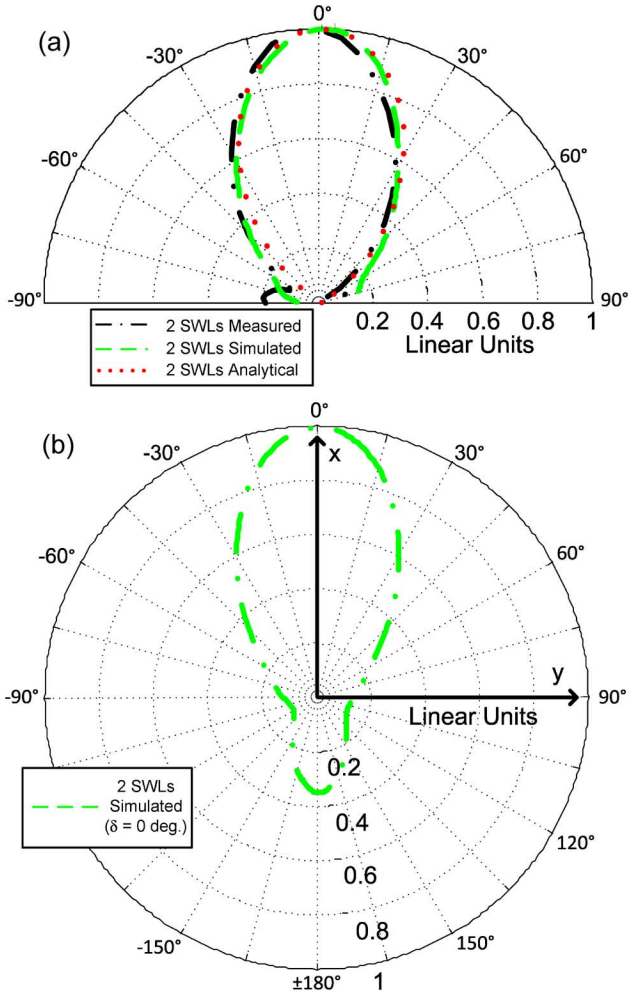

Fig. 7. Normalized polar plot of the SW beam pattern of the two-element array of SWLs (shown in linear units) with no phase variation between elements ($\delta = 0°$). Results are in good agreement. (a) Measured, simulated, and analytical beam patterns in the forward $+\hat{x}$ direction with the SWLs placed at the edge of the slab. (b) The back lobe SW radiation (generated by coplanar waveguide transmission line feed and tuning and reflector slots) was simulated by placing the SWLs at the center of the slab. A physical model was not realized since measured and simulated results were in good agreement for the edge placement of the SWLs as in (a).

IV. A Linear Array of Six SWLs With Nonuniform Weighting

Section III has outlined that an array of two SWLs can be modeled with analytical SW beam patterns and standard array theory. Measured, simulated and analytical results are all in good agreement and depict the SW field distribution on the GDS. This section investigates the possibility of a six-element linear array of SWLs with nonuniform weighting. Specifically, a binomial weighting distribution is utilized for minimal sidelobe levels [8]. In addition, calculated weights are determined for directing the main SW beam to a desired location (at $\phi = 30°$) using the Godara method [9]. These two examples suggest that known array theory can be applied to other configurations of SWLs for advanced SW beam steering.

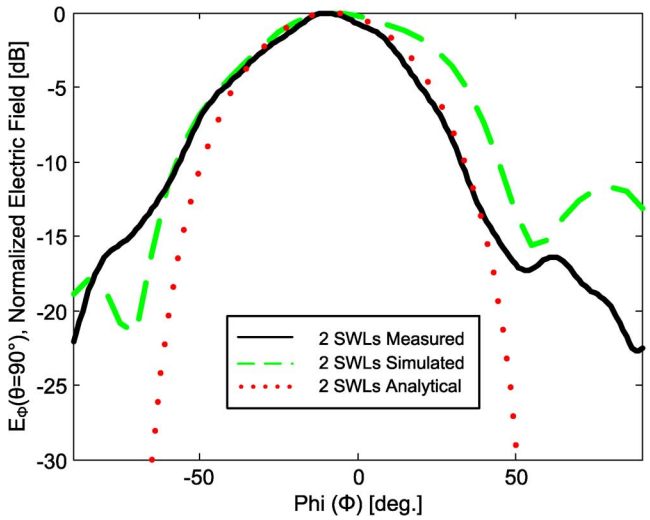

Fig. 8. Normalized SW beam pattern of the two-element array of directive SWLs shown in dB with a $+30°$ phase variation between elements. An 8° shift in the main beam is observed. Sidelobes are developed 12 dB below the main beam and 75 ° away from the main beam.

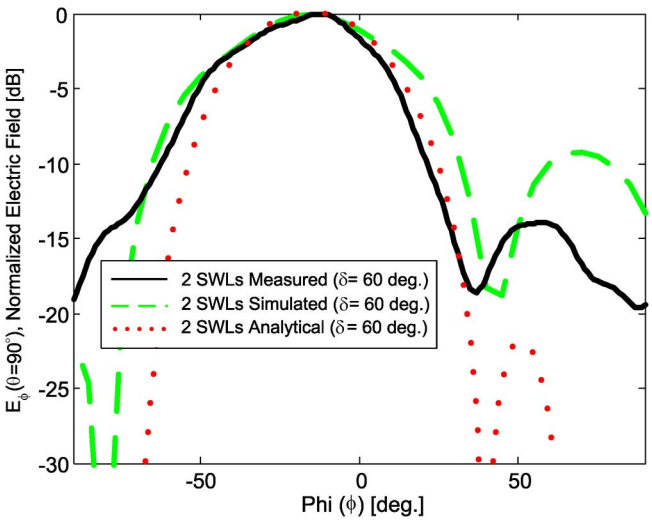

Fig. 9. Normalized SW beam pattern of the two-element array of directive SWLs shown in dB with a $+60°$ phase variation between elements. A 12.5 ° shift in the main beam is observed. Sidelobes are developed 10 dB below the main beam and 87 ° away from the main beam.

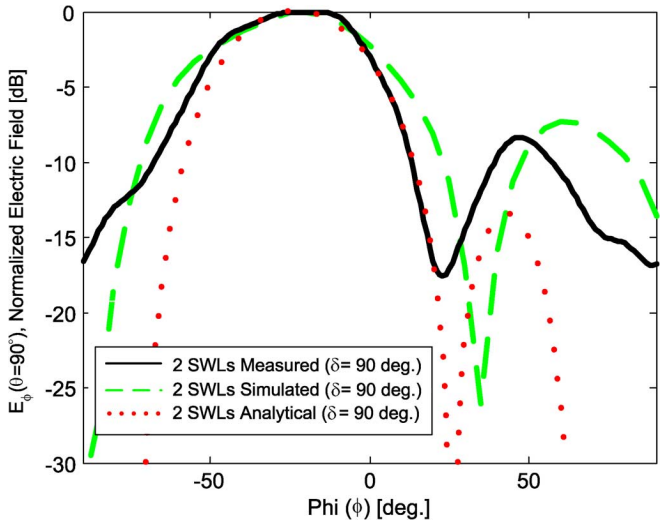

Fig. 10. Normalized SW beam pattern of the two-element array of directive SWLs shown in dB with a $+90°$ phase variation between elements. A 18 ° shift in the main beam is observed. Sidelobes are developed 7 dB below the main beam and 102 ° away from the main beam.

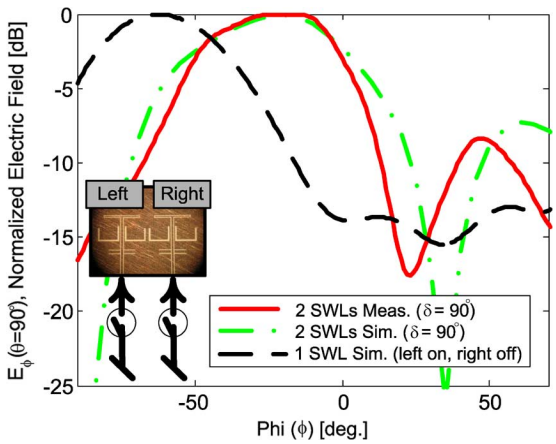

Fig. 11. Results for the left SWL turned on and the right SWL turned off (right/left description as displayed in the inset of the above figure). Simulated SW beam pattern and comparison to both SWLs on (with $\delta = 90°$). The main SW beam is steered to $\phi = -60°$ with reduced sidelobe levels.

A. Binomial Distribution

Binomial weighting in a linear array can create an array factor with no sidelobes [8], provided that the element spacing is $d \leq \lambda^{SW}/2$. Such a weighting distribution was applied to the aforementioned six-element array of directive SWLs. The normalized binomial weights were chosen from the sixth row of Pascal's triangle. They are as follows: $w_1 = w_6 = 0.1$, $w_2 = w_5 = 0.5$, and $w_3 = w_4 = 1.0$ (where the elements are labeled left to right). The total analytical beam pattern can be defined by (3), where the array factor is

$$AF(\phi) = \sum_{n=1}^{6} w_n \cos\left(\frac{2n-1}{2}\pi \sin\phi\right). \tag{4}$$

The analytical SW beam pattern is compared to the simulated (as shown in Fig. 12) and results are in good agreement.

B. Fixed Weight Beam Forming

The Godara method [9] provides a design formula to calculate the nonuniform weights required to steer a main beam and place nulls at desired locations. If the main SW beam is positioned at $\phi = 30°$ and nulls are desired at $\phi = 0°$ and $\phi = -45°$ the normalized weights are as follows:

$$\begin{aligned} w_1 &= 0.62e^{-j193.6°},\ w_2 = 0.84e^{-j85.4°} \\ w_3 &= 1.00e^{+j15.1°},\ w_4 = 1.00e^{+j74.9°} \\ w_5 &= 0.84e^{+j175.4°},\ w_6 = 0.61e^{+j283.6°}. \end{aligned} \tag{5}$$

If the array factor is determined by (4) with weights described by (5) and an element factor dictated by (1), the analytical SW beam pattern can be calculated. A good agreement is achieved between the simulated SW beam pattern and the analytical

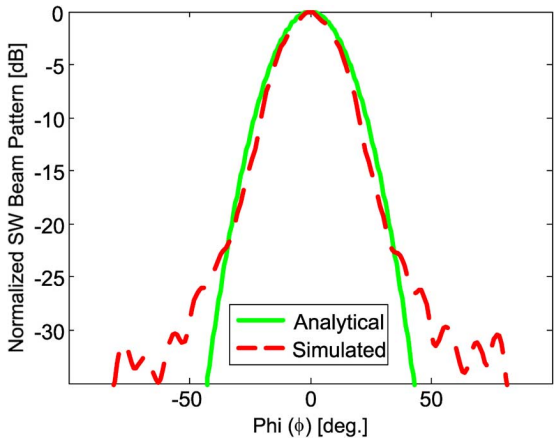

Fig. 12. Analytical and simulated SW beam patterns for a six-element array of SWLs (spacing $d = \lambda^{SW}/2$). As expected the binomial weighting distribution achieves no sidelobes in both the simulated and analytical beam patterns.

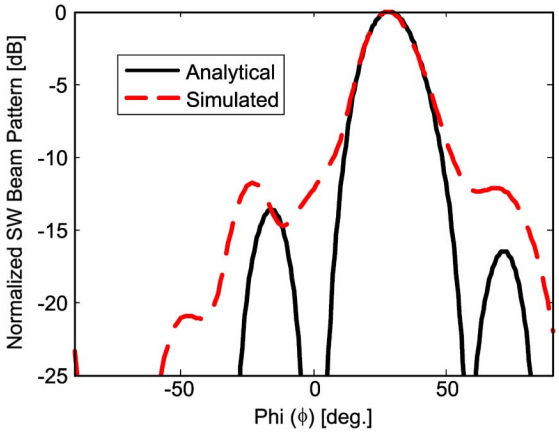

Fig. 13. Analytical and simulated SW beam patterns for a six-element array of SWLs (spacing $d = \lambda^{SW}/2$). The main beam is steered to $\phi = 30°$ and nulls are placed at $\phi = 0°$ and $\phi = -45°$.

model as shown in Fig. 13. Both main beams are steered to $\phi = 30°$. Nulls are positioned at $\phi = 0°$ and $\phi = -45°$ for the analytical model and $\phi = 5°$ and $\phi = -45°$ for the simulated SWL array. The first sidelobe (less than 10 dB from main lobe) appears at $\phi = 10°$ and $\phi = 15°$ for the analytical and simulated SW beam patterns, respectfully.

V. A Technique to Measure the SW Fields and, Hence, the SW Beam Patterns

To observe the evanescent SWs generated by the SWLs, measurements were completed and compared against simulated and analytical values for a single SWL and the two-element array. This section explains the measurement technique employed (and analogous simulation procedure) to determine the field distribution and, hence, SW beam patterns on top of the GDS [10]. Results are shown in Figs. 4, 7–11.

Essentially, the steered SW beam patterns were measured by a near-field probe in 5° steps (on top of the GDS) on an arc centered (radius $r_0 = 4.5$ cm and $r_0 \gg \lambda^{SW}$) at the SWL elements. Specifically, the single SWL element was placed in the center of the ground plane of the slab while the SWL array was placed at the edge of the high permittivity substrate (board size:

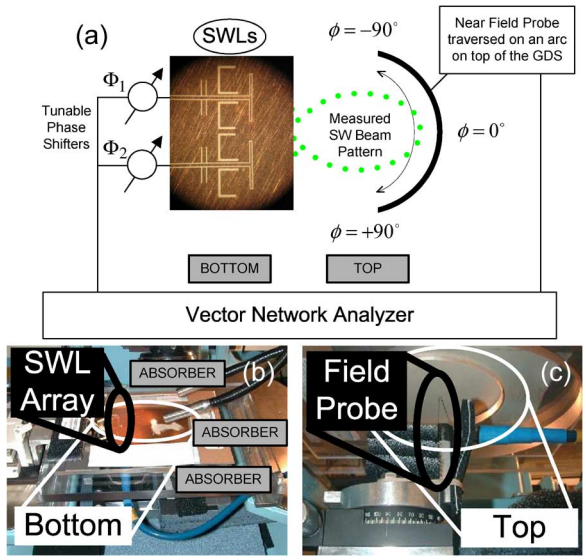

Fig. 14. Surface-wave beam pattern measurement system. (a) A near-field probe (on top of the GDS and 0.5 mm above the air-dielectric interface) was used to measure the evanescent SW field distribution along the edge of an arc on the guiding surface. The system was connected to a VNA for measurement recording. (b) The SWLs were excited (on the bottom) and absorber was used to minimize reflections. (c) The probe was mounted on a modified rotation stage and the SW beam patterns were measured on the GDS (top).

15 cm × 15 cm). For the SWL array the SW beam was controlled by adjusting the phase at the input of the SWL elements using a mechanical phase shifter (see Fig. 14).

The measured fields along this arc represent the SW field distributions at a significant distance from the SWL antenna source and thus can represent the SW beam pattern on the GDS. In addition, the raw measurements were aperture gated (to eliminate multiple reflections from the edges of the guiding structure and unwanted image sources) and time gated (to minimize high frequency noise, multiple reflections due to cable bending and field probe discontinuities from VNA measurements) as described in [18] and [19].

VI. A Specific Antenna Application for Single Frequency LW Beam Steering

If a 2-D continuous metallic grating is placed a suitable distance from the two-element SWL array (and on top of the GDS) LWs can be excited. The printed metallic grating, defines an effective PRS and LW radiation is achieved by a fast $n = -1$ spatial harmonic. Curvilinear gratings are optimal since the periodic metallic strips are conformal to the phase front generated by the SWLs [4]. Such a 2-D LWA can excite backward or forward cylindrical LWs generating pencil and conical-sector beam patterns for specified scan angles [3]–[6].

Physically, the guided TM_0 SW mode becomes perturbed by the addition of the continuous strip gratings and the bound SWs are diffracted. The propagating SW on the aperture inductively couples to the strips and the current distribution (on the strips) radiates and defines the far-field beam pattern. Essentially, suitable conditions are appropriate for TM_z cylindrical LW excitation on the guiding surface. The cylindrical LW modes are of order $n \geq 1$, since the generated far-field beam patterns have

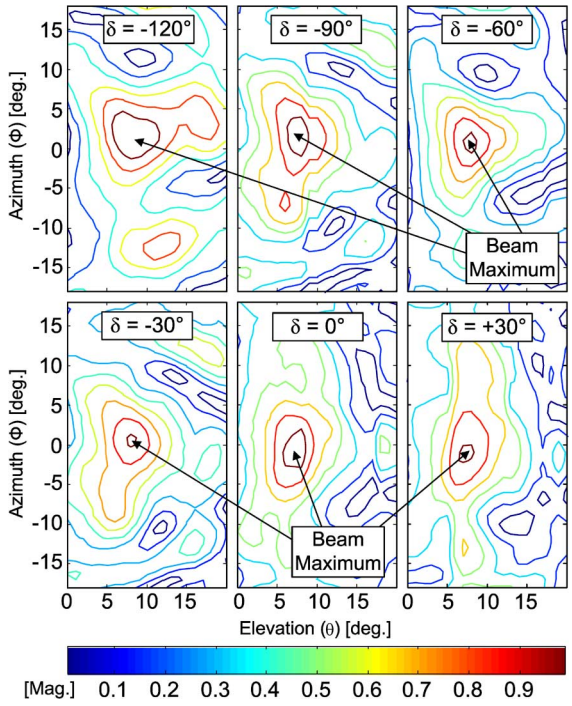

Fig. 15. Measured gain E_θ in the far field. Shown in linear units and normalized for the elliptical grating at 21.61 GHz with $\delta = -120°$, $-90°$, $-60°$, $-30°$, $0°$, and $+30°$.

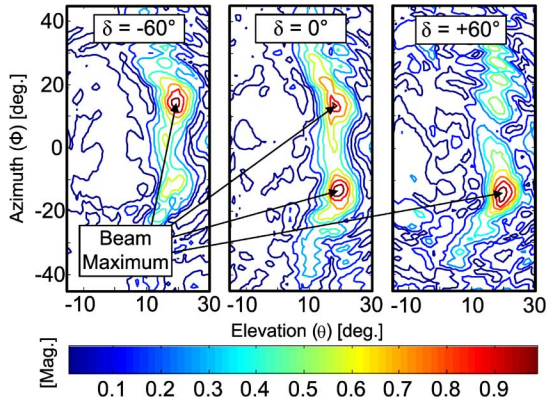

Fig. 16. Measured gain E_θ in linear units and normalized for the elliptical grating at 22.54 GHz with $\delta = -60°$, $0°$, and $+60°$.

a $\hat{\phi}$ dependence. In general, multiple types of LW modes (related to the specific PRS configuration) can exist on 2-D planar guiding surfaces and hence the total beam pattern is related to the superposition of these individual LW field distributions on the aperture [20].

Since the steered SW fields from the SWL array are directed within a certain region on top of the GDS, the cylindrical LWs are contained within a specified region as well. The LW fields within this region are similar in nature to full cylindrical TM_z LW modes but with an obvious $\hat{\phi}$ dependence. Essentially, the steered SW field distribution dictates the region of LW field excitation demonstrating single frequency conical-sector beam steering in the far field.

A. Continuous Elliptical Gratings

The investigated LWA is shown in Fig. 2 and is defined by an elliptical grating. A vector function $f_m\langle x\rangle$ can be defined to describe the curvature of the mth concentric ring (in mm)

$$f_m\langle x\rangle = 19\left(1+\frac{(m-1)}{2}\right)\sqrt{1-\frac{x^2}{19\left(1+\frac{(m-1)}{2}\right)^2}} \quad (6)$$

where the separation between each ring is 6 mm and the thickness of the strips is 1.25 mm [17].

B. Measured LW Beam Patterns

Measured 2-D beam patterns for the continuous elliptical strip grating are shown in Figs. 15 and 16 at 21.61 and 22.54 GHz, respectively. Results are normalized and shown in linear units and the far-field beam pattern measurement technique is further described in Section VI-D. At 21.61 GHz the main conical-sector beam traces the path of a narrow cone from $\phi \in [+4°, -1°]$ at $\theta = 7°$ with an element tunning range of $\delta = -120°$, $-90°$, $-60°$, $-30°$, $0°$ and $+30°$. Minor beam steering is observed at this frequency since the generated pencil beam is very close to broadside. In addition, since the design is completely symmetric, it is expected that for $\delta \in [-120°, +120°]$ the main beam will be contained within $\phi = [+4°, -4°]$ at $\theta = 7°$. Furthermore, for $\delta = -120°$ a secondary beam is clearly observed at $\theta = 12°$ and $\phi = -12°$ due to increased SW sidelobe power levels.

As expected with this LWA, with an increase in frequency the main beam scans towards end fire and an increase in the azimuth steering range is possible as shown in Fig. 16. An interesting result is observed with this elliptical grating for increased frequencies (21.72 GHz $\leq f \leq$ 23.78 GHz). At 22.54 GHz and for $\delta = 0°$, the main conical-sector beam is split into two distinct pencil beams at $\theta = +19°$ and $\phi = \pm 13°$. While for $\delta = -[+]60°$ the main beam is located at $\theta = +19°$ and $\phi = +[-]13°$. It should be noted that side lobes are observed 6 dB below the main pencil beam for relative phase differences of $\pm 60°$ between SWL elements.

Thus, these results from the preliminary elliptical design are indeed promising. With appropriate PRS design, efficient single frequency LW beam steering can be realized with further pencil beam control and reduced sidelobe levels.

C. General Discussion

These results suggest that multiple LW modes can exist on this specific elliptical grating (which has similarities to that of the straight grating [21]) as a function of frequency and azimuth and that total beam pattern in the far field is the superposition of multiple beam patterns [20]. For example, with $\delta = -[+]60°$ the main beam is located at $\phi = +[-]13°$ and a secondary beam is observed with significantly less magnitude at $\phi = -[+]13°$. Thus, the strength of the LW field excitation is dependant on the direction of propagation of the guided-wave mode along the aperture (which is steered and excited by the two-element SWL array) and that two distinct beam patterns can be generated in the far field from this elliptical grating.

D. Measurement Technique for the 2-D Gain Patterns

The 2-D far-field beam patterns were determined by measuring the elliptical grating LWA in an anechoic chamber. A

mechanical phase shifter (phase slope $\leq 3^\circ/\mathrm{GHz}$) was calibrated at 21.5 GHz achieving the varied phase differences between the two SWL elements. Gain measurements were conducted over a broad frequency span of interest, 18–24 GHz (using an Anritsu 37377C VNA with 201 data points), while the LWA was translated in the azimuth and elevation (using a Newport ESP7000 Universal Motion Controller) in 1° increments for $\theta \in [-15^\circ, +35^\circ]$ and $\phi \in [-90^\circ, +90^\circ]$. Sample results were plotted in elevation and azimuth (with contour defining gain) as shown in Figs. 15 and 16.

VII. Conclusion

An array of SWLs has been demonstrated. By varying the relative phase difference between a pair of directive SWLs, on the bottom of a GDS, bound SWs can be steered. By a $\pm 90^\circ$ relative phase difference between SWL elements, a shift of 18° in the position of the main SW beam was realized. Measured, simulated and analytical SW beam patterns are in good agreement.

A six-element linear array of SWLs with nonuniform weighting was also developed. A binomial distribution was utilized for minimal sidelobe levels in the main SW beam. Calculated weights were also determined for directing the main SW beam to a desired location at $\phi = 30^\circ$. This extension of the two-element SWL design suggests that known array theory can be applied to other complex SWL arrays for single frequency SW, and furthermore, LW beam steering structures.

Specifically, with the addition of periodic metallic gratings (on top of the GDS and using the two–element SWL array) cylindrical LWs can be steered. A continuous elliptical grating configuration was presented and measured beam patterns are shown at 21.61 and 22.54 GHz. At 21.61 GHz, the beam is contained within $\phi = [+4^\circ, -4^\circ]$ at $\theta = 7^\circ$ for a $\pm 120^\circ$ relative phase difference between SWLs. With an increase in frequency the main pencil beam scans toward endfire with an increased steering range in the azimuth. At 22.54 GHz, the main conical-sector beam splits into two distinct pencil beams located at $\theta = +19^\circ$ and $\phi = \pm 13^\circ$. Such a SWL array can be applied to other grating configurations for novel single frequency LW beam steering antennas.

References

[1] S. Mahmoud, Y. M. M. Antar, H. Hammad, and A. Freundorfer, "Theoretical considerations in the optimization of surface waves on a planar structure," *IEEE Trans. Antennas Propag.*, vol. 52, no. 8, pp. 2057–2063, Aug. 2004.

[2] H. Hammad, Y. M. M. Antar, A. Freundorfer, and S. Mahmoud, "Uniplanar CPW-fed slot launchers for efficient TM0 surface wave excitation," *IEEE Trans. Microw. Theory Tech.*, vol. 51, no. 4, pp. 1234–1240, Apr. 2003.

[3] M. Ettorre, S. Bruni, G. Gerini, A. Neto, N. Llombart, and S. Maci, "Sector PCS-EBG antenna for low-cost high-directivity applications," *IEEE Antennas Wireless Propag. Lett.*, vol. 6, pp. 537–539, 2007.

[4] S. K. Podilchak, A. P. Freundorfer, and Y. M. M. Antar, "Planar leaky-wave antenna designs offering conical-sector beam scanning and broadside radiation using surface-wave launchers," *IEEE Antennas Wireless Propag. Lett.*, vol. 7, pp. 155–158, 2008.

[5] S. K. Podilchak, A. P. Freundorfer, and Y. M. M. Antar, "New planar antenna designs using surface-wave launchers for controlled leaky-wave beam steering (invited paper)," presented at the APS-URSI, San Diego, CA, Jul. 2008.

[6] S. K. Podilchak, A. P. Freundorfer, and Y. M. M. Antar, "Directive and nondirective surface-wave launchers and application to broadside radiation and beam steering leaky-wave antennas," presented at the URSI, Chicago, IL, Aug. 2008.

[7] D. M. Pozar, *Microwave Engineering*, 3rd ed. Hoboken, NJ: Wiley, 2005.

[8] C. A. Balanis, *Antenna Theory*, 3rd ed. Hoboken, NJ: Wiley, 2005.

[9] L. Godara, "Application of antenna arrays to mobile communications, Part II: Beam-forming and direction of arrival considerations," *Proc. IEEE*, vol. 85, no. 8, pp. 1195–1245, Aug. 1997.

[10] A. P. Freundorfer, M. Z. I. Bekheit, and Y. M. M. Antar, "Measurements of a Compact surface wave launcher array with application to single frequency beam steering leaky wave antennas," presented at the Asia-Pacific Microw. Conf., Dec. 2006.

[11] P. Baccarelli, P. Burghignoli, G. Lovat, and S. Paulotto, "Novel microstrip leaky-wave 'bull-eye' antenna with suppressed surface-wave excitation," in *Tech. Dig. IEEE AP-S Symp. Antennas Propag.*, 2004, vol. 1, pp. 1078–1081.

[12] N. Llombart, A. Neto, G. Gerini, and P. de Maagt, "Planar circularly symmetric EBG structures for reducing surface waves in printed antennas," *IEEE Trans. Antennas Propag.*, vol. 53, no. 10, pp. 3210–3218, Oct. 2005.

[13] A. Neto, N. Llombart, G. Gerini, and P. de Maagt, "On the optimal radiation bandwidth of printed slot antennas surrounded by EBGs," *IEEE Trans. Antennas Propag.*, vol. 54, no. 4, pp. 1074–1083, Apr. 2006.

[14] N. Llombart, A. Neto, G. Gerini, and P. De Maagt, "1-D scanning arrays on dense dielectrics using PCS-EBG technology," *IEEE Trans. Antennas Propag.*, vol. 55, no. 1, pp. 26–35, Jan. 2007.

[15] D. Sievenpiper, J. Colburn, B. Fong, J. Ottush, and J. Visher, "Holographic artificial impedance surfaces for conformal antennas," in *Proc. Antennas Propag. Soc. Int. Symp.*, Jul. 3–8, 2005, vol. 1B, pp. 256–259.

[16] A. Ip and D. R. Jackson, "Radiation from cylindrical leaky waves," *IEEE Trans. Antennas Propag.*, vol. 38, no. 4, pp. 482–488, Apr. 1990.

[17] M. Bekheit, "A new scanning metallic grating antenna utilizing a novel scanning technique at 24 GHz," Masters Thesis, Queen's Univ., Kingston, ON., Canada, Jan. 2005.

[18] M. Sjostrom, "Properties of smoothing with time gating," in *Proc. ISCAS 2000* , May 2000, vol. 1, pp. 707–710.

[19] Y. T. Hsiao, Y. Y. Lin, Y. C. Lu, and H. T. Chou, "Applications of time-gating method to improve the measurement accuracy of antenna radiation inside an anechoic chamber," *Proc. AP-S. Dig.*, vol. 3, no. 4, pp. 794–797, Jun. 2003.

[20] A. Ip and D. R. Jackson, "Radiation from cylindrical leaky waves," *IEEE Trans. Antennas Propag.*, vol. 38, no. 4, pp. 482–488, Apr. 1990.

[21] P. Baccarelli, P. Burghignoli, F. Frezza, A. Galli, P. Lampariello, G. Lovat, and S. Paulotto, "Modal properties of surface and leaky waves propagating at arbitrary angles along a metal strip grating on a grounded slab," *IEEE Trans. Antennas Propag.*, vol. 53, no. 1, pp. 36–46, Jan. 2005.

Symon K. Podilchak (S'03–M'05) received the B.A.Sc. degree from the University of Toronto, ON, Canada, in 2005.

His current research interests include the analysis and design of planar leaky-wave antennas, metamaterials, millimeter-wave CMOS integrated circuits, and periodic structures. He is currently working toward the Ph.D. degree at Queen's University, Kingston, ON, and the Royal Military College of Canada. He has also had experience as a computer programmer, technology investment analyst, and assisted in the design of radomes for 77–GHz automotive radar. Recent industry experience also includes modeling the radar cross section of military vessels for high frequency surface-wave radar.

Mr. Podilchak received the Young Scientist Award for the XXIX General Assembly of the International Union of Radio Science (URSI) in Chicago, in 2008.

Al P. Freundorfer (M'90) received the B.A.Sc., M.A.Sc., and Ph.D. degrees from the University of Toronto, ON, Canada, in 1981, 1983, and 1989, respectively.

In 1990, he joined the Department of Electrical Engineering, Queen's University, Kingston, ON, Canada. Since then, he has done work in nonlinear optics of organic crystals, coherent optical network analysis, as well as microwave integrated circuits. Currently, he is focusing his attention on monolithic microwave circuits used in lightwave systems with bit rates in excess of 20 Gb/s and on monolithic millimeter wave integrated circuits used in wireless communications.

Yahia M. M. Antar (S'73–M'76–SM'85–F'00) was born on November 18, 1946, in Meit Temmama, Egypt. He received the B.Sc. (Hons.) degree from Alexandria University, Egypt, in 1966, and the M.Sc. and Ph.D. degrees from the University of Manitoba, Winnipeg, Canada, in 1971 and 1975, respectively, all in electrical engineering.

In 1966, he joined the Faculty of Engineering, Alexandria University, where he was involved in teaching and research. At the University of Manitoba, he held a University Fellowship, an NRC Postgraduate and Postdoctoral Fellowships. From 1976 to 1977, he was with the Faculty of Engineering, University of Regina. In June 1977, he was awarded a Visiting Fellowship from the Government of Canada to work with the Communications Research Centre, Department of Communications, Shirley's Bay, Ottawa, where he was involved in research and development of satellite technology with the Space Electronics group. In May 1979, he joined the Division of Electrical Engineering, National Research Council of Canada, Ottawa, where he worked on polarization radar applications in remote sensing of precipitation, radio wave propagation, electromagnetic scattering, and radar cross-section investigations. In November 1987, he joined the staff of the Department of Electrical and Computer Engineering, Royal Military College of Canada, Kingston, ON, Canada, where he is now a Professor of electrical and computer engineering. He holds adjunct appointment with the University of Manitoba, and has a cross appointment with Queen's University in Kingston. He has authored or coauthored more than 140 journal papers on these topics, and supervised or cosupervised more than 50 Ph.D. and M.Sc. theses at the Royal Military College and Queen's University, of which four have received the Governor General Gold Medal. His current research interests include polarization studies, integrated antennas, microwave, and millimeter wave circuits.

Dr. Antar's recent professional activities and awards include election to the Engineering Institute of Canada (FEIC) as a Fellow, and in 2003, he received RMC's Excellence in Research Prize. In May 2002, he became the holder of a Canada Research Chair (CRC) in Electromagnetic Engineering. He served as an Associate Editor of the IEEE TRANSACTIONS ON ANTENNAS AND PROPAGATION and is an Associate Editor (Features) of the IEEE ANTENNAS AND PROPAGATION MAGAZINE. He is presently a Vice-President of International Scientific Radio Union (URSI) and was the previous Chairman of the URSI Canadian National Commission (CNC).